Bol. Soc. Paran. Mat.
©SPM – E-ISSN-2175-1188
SPM: www.spm.uem.br/bspm

(3s.) **v. 2026 (44) 12** : 1–16.
ISSN-0037-8712
doi:10.5269/bspm.81818

# Mhd Natural Convection with Radial Heat and Mass Transfer Under Heat and Mass Absorption in a Vertical Annulus

Muhammad Yusuf Muhammad*, Yusuf Y. Gambo, Muhammad Auwal Lawan Mukhazah, Ado Balili and Auwalu Alhassan Girema

ABSTRACT: This study presents an analytical investigation of the combined effects of an applied radial magnetic field, an induced magnetic field, and inverse-square heat and mass absorption on fully developed natural convection flow of laminar, viscous incompressible electrically conducting fluid. The governing equations are formulated non-dimensionally and solved analytically under steady-state conditions. Key dimensionless parameters, such as the Hartmann number (Ha), heat absorption parameter (S), chemical reaction parameter ($K^*$) and annular gap ratio ($\lambda$), are systematically varied to examine their effects on velocity, temperature, concentration, magnetic field, and induced current density distributions. The results indicate that increasing Hartmann number suppresses velocity due to Lorentz force effects while enhancing the magnetic field intensity. The annular gap $\lambda$ significantly influences flow dynamics, enhancing heat and mass transfer. Higher heat absorption decreases velocity and temperature, confirming its role in energy extraction, while an increase in ($K^*$) depletes concentration as a result of accelerated species diffusion. Furthermore, isothermal boundary conditions exhibit higher distributions profiles compared to iso-flux conditions, demonstrating improved convective transport. The numerical results indicate that increasing Ha generally decreases skin friction, attributed to the Lorentz force. Under isothermal conditions, higher Ha leads to a decline in $\tau_\lambda$ and Q, while for the iso-flux case, $J_\theta$ shows irregular variations, including negative values suggesting a current reversal. Increasing the annular gap ($\lambda$) raises skin friction. Nusselt number (Nu), decreases with increasing $\lambda$, but increases with higher S, indicating that heat absorption promotes efficient convective transport. Isothermal conditions show more effective heat transfer than iso-flux conditions. The ratio of the mass transfer coefficient (Sh) goes down as $\lambda$ goes up and goes up as ($K^*$) goes up. The iso-flux condition consistently produces lower Sherwood numbers, which means that mass transfer is less effective. These findings offer essential insights for enhancing MHD-driven thermal and mass transport systems, applicable in electromagnetic propulsion, nuclear reactor cooling, and advanced energy conversion technologies.

Keywords: Magnetohydrodynamics (MHD), natural convection, vertical concentric annulus, heat absorption, mass transfer, Hartmann number, thermal transport.

## Contents



* Corresponding Author.
2020 *Mathematics Subject Classification:* 76W05, 76R10, 80A20.
Submitted February 02, 2026. Published April 21, 2026

## 1. Introduction

The study of Magnetohydrodynamics (MHD) natural convection in vertical concentric annuli has received significant attention due to its broad implications in engineering, energy systems, and industrial processes. These circular shapes are simple models that help us learn about complex thermal and fluid transport phenomena, especially when magnetic fields and electrically conductive fluids come together.

It is important to understand how natural convection, heat and mass generation/absorption, and magnetic field effects interact to improve activities like cooling nuclear reactors, utilizing electromagnetic propulsion, producing energy from geothermal sources, and undertaking metallurgical activity. A radial magnetic field and induced currents in an annular space modify the way fluids and heat move in highly complex ways. This has a significant effect on MHD power generation, solidification processes in metal casting, and advanced cooling technologies.

There has been increasing interest in mathematical analysis and closed form solutions of MHD flow in vertical annuli since they are becoming more significant in cooling systems and enhancing heat transfer. Previous studies have looked at natural convection in vertical annuli with isothermal and iso-flux conditions in great detail. For example, [11] used analytical methods to look at how heat sources and sinks and induced magnetic fields affect natural convection flow in vertical concentric annuli when there is a radial magnetic field. In the same way, [17] looked into how natural convection along a vertical coaxial cylinder with a constant heat flow at the inner wall affects heat absorption.

An induced magnetic field's effect on fully developed convection flow in an annular micro-channel was studied in [9]. The development of natural convection in an open-ended vertical annulus with a rotating inner cylinder was studied in [3] using the implicit finite difference (IFD) method. Their results showed that heating the inner cylinder made the flow more stable, whereas heating the outside cylinder made the flow less stable.

Studies by [21] and [10] built on this by looking at free convection in open-ended pipes and fully developed free convection in vertical annuli under different boundary conditions. The dynamics of electrically conductive fluids in MHD systems is of importance due its significance in power generation and battery technology. Prior studies, such as that of [23], established the basis for understanding these fluids. [22] examined the flow between two spinning concentric cylinders in a radial magnetic field, determining that the velocity was continuously diminished in the magnetic field compared to the hydrodynamic scenario. [1] subsequently investigated MHD flow between coaxial spinning cylinders, yielding divergent results that underscored the intricate relationship between magnetic fields and fluid dynamics.

More recently, [24] showed that while the temperature is constant, both the velocity and the strength of the induced magnetic field are much larger than when the heat flux is constant. The growing need for precise regulation of heat transfer has led to a lot of research into fluids that generate heat (sources) and fluids that absorb heat (sinks). This has resulted in a variety of mathematical models that can predict how these fluids will behave thermally. Initial theoretical models by [6] and [18] posited constant rates of heat generation and absorption, however subsequent studies by [2] and [26] integrated spatial variations in heat sources and sinks. [5,12,26] looked at how expansion and friction might cause heat to build up, while [13] suggested that heat generation and temperature are related in the other way. A widely recognized model by [4] stated that the volumetric heat source rate is proportional to the temperature differential.

Several research that came after looked at how vertical concentric cylinders generate or absorb heat [7,19,8,25,27]. Recently, [20] examined the effects of radially varying magnetic fields and thermal sources/sinks on MHD free convection in a vertical concentric annulus. Additionally, studies by [14,15,16], inspired by previous research ( [25,24,11]), offered precise solutions for natural convection flow in vertical concentric annuli subjected to radial and induced magnetic fields.

Since it's generally known that the amount of heat generated depends on changes in temperature, it's important to fully understand these interactions in order to improve the design and performance of MHD-driven thermal systems. The impact of heat absorption adds to the complexity of the thermal field by creating effects that control how warmth is spread out and how fluids move.

Even though there has been a lot of research on MHD flows in annular geometries, the effects of inverse-square heat and mass absorption, applied radial and induced magnetic fields on natural convection are still not well understood in the literature. This paper seeks to address this deficiency by examining the

governing equations of magnetohydrodynamic (MHD) natural convection in a vertical concentric annulus influenced by heat and mass absorption. It further extends the analysis to a double-diffusive convection model, providing a more comprehensive and informative perspective. We use analytical methods to look into how important factors like the Hartmann number, heat absorption parameter, and annular gap ratio affect the distributions of velocity, temperature, concentration, magnetic field, and induced current density.

## 2. Mathematical Formulation

The study setup, shown in figure 1, consists of a fully developed natural convection flow of a constant, viscous, and incompressible electrically conducting fluid inside an infinitely long vertical concentric annulus. The $z'$-axis runs vertically up along the axis of the coaxial cylinders, while the $R'$-axis runs outward from the cylinder's axis. The magnetic field that is applied from the outside, which is written as $(aH'_o)/R'$, points radially outward. Under constant conditions, $T'_i$ and $T'_a$ are the temperatures of the outer surface of the inner cylinder and the air around it, respectively. The annular zone is where the fluid flows and absorbs heat from the inside. The velocity components are denoted as $U'_{R'}$, $U'_\theta$, and $U'_{z'}$, which correspond to the radial ($R'$), azimuthal ($\theta$), and axial ($z'$) directions, respectively. The radial and azimuthal velocity components go away since the flow is fully developed, which means that $U'_{R'} = U'_\theta = 0$. Because the cylinders are infinitely long and the flow is fully developed, the flow characteristics only depend on R.

Using the Boussinesq approximation, the basic governing equations for the fluid flow in this model are written in their dimensional forms as shown in equations (2.1), (2.2), (2.3), and (2.4).

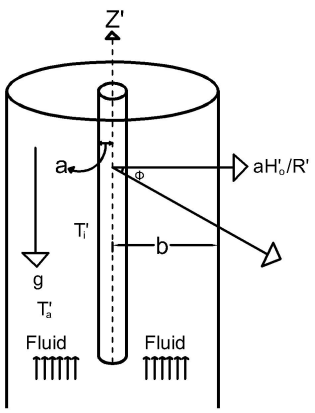


Figure 1: Geometry of the model

**Momentum Equation:**

$$\nu\left(\frac{d^2U'}{dR'^2}+\frac{1}{R'}\frac{dU'}{dR'}\right)+g\beta(T'-T'_a)+g\beta^*(C'-C'_a)+\frac{\mu_e H'_o}{\rho R'}\frac{dH'_z}{dR'}=0 \tag{2.1}$$

**Magnetic Induction Equation:**

$$\eta\left(\frac{d^2H'_z}{dR'^2}+\frac{1}{R'}\frac{dH'_z}{dR'}\right)+\frac{H'_o}{R'}\frac{dU'}{dR'}=0 \tag{2.2}$$

**Energy Equation:**

$$k\left(\frac{d^2T'}{dR'^2}+\frac{1}{R'}\frac{dT'}{dR'}\right)+\frac{Q^*_o a^2(T'-T'_a)}{\rho C_p R'^2}=0 \tag{2.3}$$

**Concentration Equation:**

$$D\left(\frac{d^2C'}{dR'^2}+\frac{1}{R'}\frac{dC'}{dR'}\right)+\frac{K'a^2(C'-C'_a)}{R'^2}=0 \tag{2.4}$$

The boundary conditions for eqns. (2.1), (2.2), (2.3), and (2.4) are as follows:

$$\begin{cases} U'=H'_z=0, \quad C'=C'_i \,/\, \dfrac{dC'}{dR'}=-\dfrac{\dot{j}'}{D}, \quad T'=T'_i \,/\, \dfrac{dT'}{dR'}=-\dfrac{\dot{q}'}{k} & \text{at } R'=a \\ U'=H'_z=0, \quad C'=C'_a, \quad T'=T'_a & \text{at } R'=b \end{cases} \tag{2.5}$$

In the above equations, the following symbols represent various physical quantities: fluid velocity $U'$, gravitational acceleration $g$, coefficient of volume expansion $\beta$, Magnetic permeability $\mu_e$, fluid density $\rho$, magnetic diffusivity $\eta$, thermal conductivity of the fluid $k$, specific heat capacity at constant temperature $C_p$, fluid temperature $T'$, fluid concentration $C'$, reaction rate $K'^*$, diffusion coefficient $D$, ambient temperature $T'_a$, heat generation/absorption parameter respectively $Q_0>0$ and $Q_0<0$.

Rendering equations (2.1)-(2.5) to the following non-dimensional variables and parameters we get:

$$R=\frac{R'}{a}, \quad U=\frac{U'}{U_o}, \quad H=\frac{H'_z}{H'_o}, \quad \theta=\frac{T'-T'_a}{T'_i-T'_a}, \quad \phi=\frac{C'-C'_a}{C'_i-C'_a}$$

$$U_o=\frac{ga^2\beta(T'_i-T'_a)}{\nu}, \quad \lambda=\frac{b}{a}, \quad Ha=a\mu_e H'_o\left[\frac{\sigma}{\rho\nu}\right]^{1/2}$$

where $Q_o=(Q^*_o a^2(T'-T'_a))/R'^2$ (radially-dependent heat generation/absorption function), $S=(Q^*_o a^2)/k$ (heat generation parameter), $K^*=(K'a^2)/D$ (chemical reaction parameter), $K=(K'a^2(C'-C'_a))/R'^2$ (radial dependent mass generation function), we obtained the following dimensionless equations:

**Dimensionless Momentum Equation:**

$$\frac{d^2U}{dR^2}+\frac{1}{R}\frac{dU}{dR}+\theta+N\phi+\frac{Ha^2}{R}\frac{dH}{dR}=0 \tag{2.6}$$

**Dimensionless Magnetic Induction Equation:**

$$\frac{d^2H}{dR^2}+\frac{1}{R}\frac{dH}{dR}+\frac{1}{R}\frac{dU}{dR}=0 \tag{2.7}$$

**Dimensionless Energy Equation:**

$$\frac{d^2\theta}{dR^2}+\frac{1}{R}\frac{d\theta}{dR}+\frac{S}{R^2}\theta=0 \tag{2.8}$$

**Dimensionless Concentration Equation:**

$$\frac{d^2\phi}{dR^2}+\frac{1}{R}\frac{d\phi}{dR}+\frac{K^*}{R^2}\phi=0 \tag{2.9}$$

**Dimensionless Boundary Conditions**

$$\begin{cases} u=H=0, \quad \chi\dfrac{d\Phi}{dR}+\gamma\Phi=\xi, \quad \chi\dfrac{d\theta}{dR}+\gamma\theta=\xi & \text{at } R=1 \\ u=H=0, \quad \Phi=0, \quad \theta=0 & \text{at } R=\lambda \end{cases} \tag{2.10}$$

Where $\chi,\gamma$ and $\xi$ are constants with $\chi=0,\gamma=1$ and $\xi=1$ for the isothermal condition, $\chi=1,\gamma=0$ and $\xi=-1$ for the isoflux condition.

## 3. Method of Solution

This study's methodology is comparable to that described in [4]. Using non-dimensional boundary conditions to solve the dimensionless governing linear simultaneous ordinary differential equations, the exact solution for the velocity, induced magnetic field, induced current density, concentration, and temperature field are obtained, along with corresponding numerical values for skin friction, Mass flux, induced current flux, Sherwood number, and Nusselt number are also obtained.

### 3.1. Analytical solution

Solving equations (2.6)-(2.9), the velocity, skin friction, mass flux, magnetic field, induced current density, induced current flux, temperature, Nusselt number, concentration, Sherwood number were determined analytically, subject to boundary conditions (2.10) as follows:

**Velocity Profile:**

$$\begin{aligned} u(R) = {} & C_1 R^{Ha} + C_2 R^{-Ha} + C_3 + D_1 R^{(2+\sqrt{S})} + D_2 R^{(2-\sqrt{S})} \\ & + D_3 R^{(2+\sqrt{K^*})} + D_4 R^{(2-\sqrt{K^*})} \end{aligned} \tag{3.1}$$

**Skin Friction**

$$\tau_1 = Ha(C_1 - C_2) + D_7 + D_8 \tag{3.2}$$

$$\tau_\lambda = -Ha(C_1 \lambda^{Ha-1} - C_2 \lambda^{-Ha-1}) + D_9 + D_{10} \tag{3.3}$$

**Mass Flux**

$$Q = 2\pi \left( \frac{C_1}{Ha+2}(\lambda^{Ha+2} - 1) + \frac{C_2}{2-Ha}(\lambda^{2-Ha} - 1) + D_{16} \right) \tag{3.4}$$

**Magnetic Field:**

$$\begin{aligned} H(R) = {} & C_4 + C_3 \ln(R) - \frac{C_1}{Ha} R^{Ha} + \frac{C_2}{Ha} R^{-Ha} - \frac{D_1}{2+\sqrt{S}} R^{2+\sqrt{S}} \\ & - \frac{D_2}{2-\sqrt{S}} R^{2-\sqrt{S}} - \frac{D_3}{2+\sqrt{K^*}} R^{2+\sqrt{K^*}} - \frac{D_4}{2-\sqrt{K^*}} R^{2-\sqrt{K^*}} \end{aligned} \tag{3.5}$$

**Induced Current Density:**

$$\begin{aligned} J_\theta = {} & C_1 R^{Ha-1} + C_2 R^{-Ha-1} + D_1 R^{1+\sqrt{S}} + D_2 R^{1-\sqrt{S}} \\ & + D_3 R^{1+\sqrt{K^\circ}} + D_4 R^{1-\sqrt{K^\circ}} - \frac{C_3}{R} \end{aligned} \tag{3.6}$$

**Induced Current Flux**

$$J = \frac{1}{Ha}(C_1(\lambda^{Ha} - 1) - C_2(\lambda^{-Ha} - 1)) + D_{24} + D_{25} \tag{3.7}$$

**Temperature Profile:**

$$\theta(R) = \frac{\xi[R^{2\sqrt{S}} - \lambda^{2\sqrt{S}} R^{-\sqrt{S}}]}{(\chi\sqrt{S} + \gamma) + (\chi\sqrt{S} - \gamma)\lambda^{2\sqrt{S}}} \tag{3.8}$$

**Nusselt Number**

$$Nu_1 = \frac{d\theta}{dR}\Big|_{R=1} = -\sqrt{S}(C_5 - C_6) \tag{3.9}$$

$$Nu_\lambda = -\frac{d\theta}{dR}\Big|_{R=\lambda} = -\sqrt{S}(C_5 \lambda^{\sqrt{S}-1} - C_6 \lambda^{-\sqrt{S}-1}) \tag{3.10}$$

**Concentration Profile:**

$$\phi(R) = \frac{\xi[R^{2\sqrt{K'}} - \lambda^{2\sqrt{K'}} R^{-\sqrt{K'}}]}{(\chi\sqrt{K'} + \gamma) + (\chi\sqrt{K'} - \gamma)\lambda^{2\sqrt{K'}}} \tag{3.11}$$

**Sherwood Number:**

$$Sh_1 = \frac{d\phi}{dR}\Big|_{R=1} = -\sqrt{K^*}(C_5 - C_6) \tag{3.12}$$

$$Sh_\lambda = -\frac{d\phi}{dR}\Big|_{R=\lambda} = -\sqrt{K^*}(C_5 \lambda^{\sqrt{K'}-1} - C_6 \lambda^{-\sqrt{K'}-1}) \tag{3.13}$$

The constants in the equations (3.1)-(3.13) are given in Appendix I.

## 4. Results and Discussion

To comprehensively analyze the fluid flow characteristics in the annular region, the governing equations were solved analytically, and the results were depicted using graphs generated by MATLAB. The primary emphasis of this study was on three significant dimensionless parameters: the heat generation parameter (S), the radii ratio ($\lambda$), and the Hartmann number (Ha). A parametric approach was employed, methodically altering each parameter while keeping others constant to identify their distinct impacts. Figures 2-19 show how these adjustments modify the flow behavior in a visual way. Also, Tables 1 and 2 show the numerical results from equations (3.2), (3.3), (3.4), (3.7), (3.9), (3.10), (3.12), and (3.13). The analysis of the Hartmann number (Ha) was conducted within a range that aligns with published research, including works by [24,11,17,20,14,15,16], thereby ensuring consistency with previous findings. Figures 2 to 19 demonstrate the complex interaction between these governing parameters. Furthermore, the study explores how the annular gap ($\lambda$), heat generation/absorption parameter (S), chemical reaction parameter ($K^*$), Hartmann number (Ha), and buoyancy ratio (N) influence the transport phenomena under boundary conditions isothermal and iso-flux.

The numerical values in Tables 3 indicate how the Hartmann number (Ha), heat absorption parameter (S), and annular gap ($\lambda$) affect skin friction ($\tau_1$ and $\tau_\lambda$), mass flux (Q), and induced current flux (J). The results show that, increasing Ha reduces skin friction. This is because the Lorentz force slows down fluid velocity. In isothermal conditions, an increase in Ha leads to a reduction in $Q$ and $J$, indicating a stabilizing effect on the flow caused by electromagnetic forces. For the iso-flux situation, though, the changes in J are less regular, and some of them are negative. This indicates that, the direction of the induced current density changes because of thermal and electromagnetic interactions. Increasing ($\lambda$) makes skin friction increases generally, for instance, at $\lambda = 3$. This demonstrates how geometry affect flow dynamics. The ($\mathrm{Nu}_1$ and $\mathrm{Nu}_\lambda$) in Table 1 shows that, thermal performance are declining as $\lambda$ widen. This implies that a larger circular gap reduces thermal conduction, resulting in reducing the values of Nu. Moreover the results indicate that, increasing heat absorption parameter (S) increases the Nusselt number under both boundary conditions. This is especially true when the temperature is constant, which means that heat absorption enhances the efficiency of convective transport. The isothermal and iso-flux situations shows that heat transfer is effective when the temperature differences are stronger, which enhances the convection.

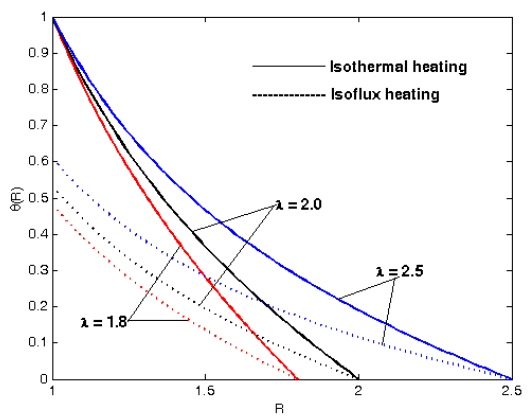


Figure 2: Temperature profile for different values of $\lambda$ at $S = 2$

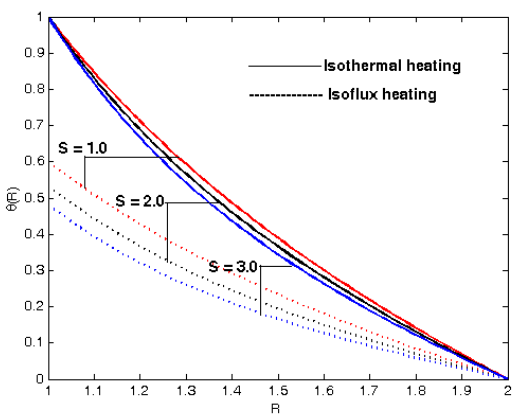


Figure 3: Temperature profile for different values of $\lambda$ at $S = 1$

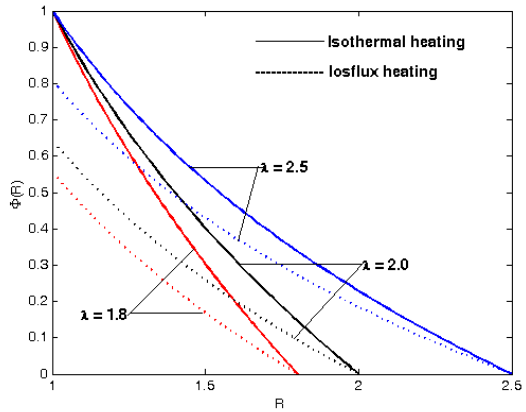


Figure 4: Concentration profile for different values of $\lambda$ at $K^* = 0.5$

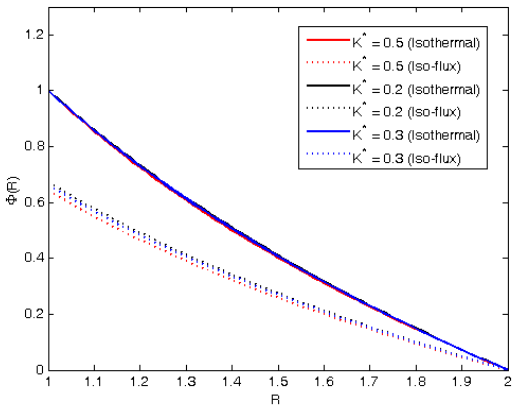


Figure 5: Concentration profile for different values of $K^*$ at $\lambda = 2$

The mass transfer dynamics, as shown in Table 2 by the Sherwood number ($\mathrm{Sh}_1$ and $\mathrm{Sh}_\lambda$), show that when $\lambda$ goes up, the $Sh$ values go down. This shows that the efficiency of mass transfer is getting worse since the two things are getting farther apart. The reaction rate ($K^*$) has a significant impact. Increasing the values of $K^*$ enhances mass transfer, especially when the temperature is maintained. This behavior is expected because chemical reactions change concentration gradients, which in turn changes diffusion speeds. Also, the iso-flux condition always gives lower Sherwood numbers, which supports the idea that mass transfer doesn't work as well when the flux is constant.

Figures 2 and 3 analyze the temperature distribution for varying $\lambda$ and S values, respectively. A larger annular gap leads to an increased temperature profile due to enhanced heat transfer efficiency. Similarly, higher values of S reduce the temperature distribution, as greater heat absorption extracts thermal energy from the system. The difference between isothermal and iso-flux conditions is more pronounced in temperature distribution, with isothermal conditions exhibiting a steeper thermal gradient. Figures 4 and 5 show the impact of $\lambda$ and $K^*$ on concentration distribution, an increase in $\lambda$ enhances concentration diffusion, indicating improved mass transfer efficiency in a wider annular gap. Conversely, increasing $K^*$ results in a reduction in concentration due to accelerated chemical reactions that deplete the reacting species. The observed trends align with theoretical expectations of mass transport in chemically reacting flows.

Figures 6 and 9 show how the Hartmann number (Ha) affects velocity. The findings show that the speed goes down as Ha goes up. This is because of the magnetic dampening effect. This behavior is in line with the well-known rule that Lorentz force is weaker in conducting fluids. When Ha is higher, electromagnetic resistance is stronger, which slows down the fluid a lot. Also, when we compare isothermal and iso-flux conditions, we see that heat flux boundary circumstances give us a lower velocity profile. The changes seen in figure 9 are in line with what other research have found (e.g., [24]). Figures 7 show how the annular gap ($\lambda$) affects the speed distribution.

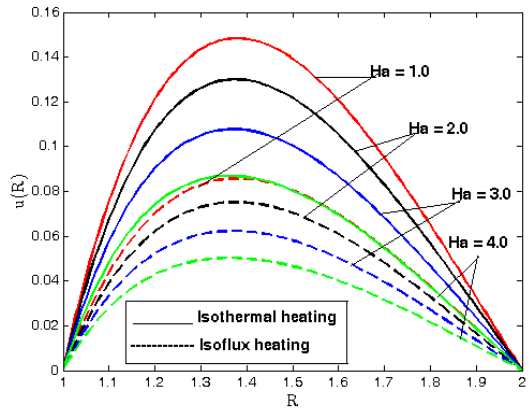


Figure 6: Velocity profile at different values of $Ha$ at $\lambda = 2, S = 2, N = 1$ and $K^* = 1$

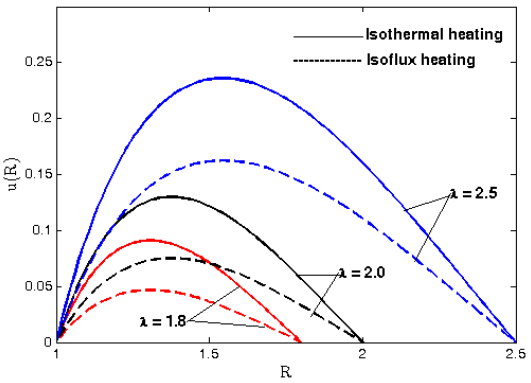


Figure 7: Velocity profile at different values of $\lambda$ at $S = 2, N = 1, K^* = 1$ and $Ha = 2$

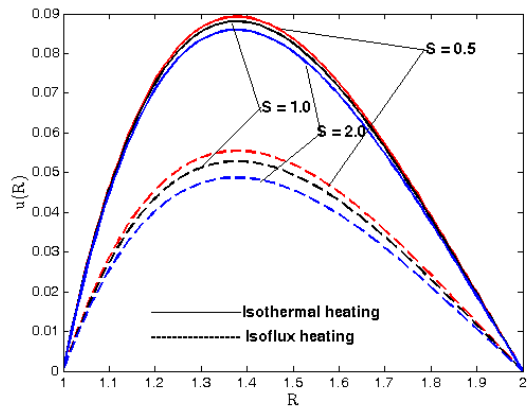


Figure 8: Velocity profile for different values of $S$ and $\lambda = 2, N = 1, K^* = 1$ at $Ha = 2$

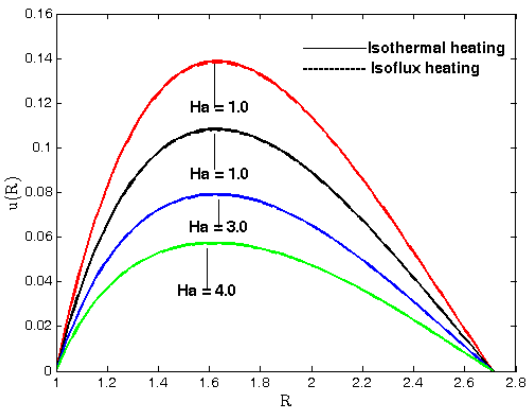


Figure 9: Velocity profile for different values of $Ha$ at $\lambda = 2.71, S \to 0, K^* \to 0$ and $N = 0$

When $\lambda$ goes up, the velocity increases also. This is because a bigger annular gap lowers flow resistance and makes it easier for fluids to move. This impact is more evident at higher radii because to the greater fluid volume available for circulation. The increase in velocity is greater when the temperature is constant than when the flux is constant. This shows how important heat transfer mechanisms are in changing velocity.

Figures 8 show how the velocity changes when $S$ changes. As $S$ increases, the fluid loses energy, which makes it move more dense. The effect is stronger for wider $\lambda$, where heat absorption is at its peak. When heating isothermal, S has a bigger influence than when heating isoflux. Figures 10 to 14 demonstrate the variations in $H(R)$ corresponding to changes in $Ha$. The results demonstrate that increasing Ha enhances the induced magnetic field, supporting theoretical projections of stronger electromagnetic coupling. The comparisons of isothermal and iso-flux conditions reveal that isothermal heating has a stronger magnetic field profile. This indicates that thermal boundary conditions influence the distribution of the induced magnetic field. The discrepancies illustrated in figure 14 correspond with findings from previous studies (see, for instance, [24]). Figures 15 to 19 show how the density of the generated current changes with Ha. The statistics demonstrate that the current density rises at initially with Ha, but then it starts to change

at higher values. The Lorentz force and the electric field that is made cause the oscillation. Isothermal boundary condition results in an elevated induced current density, highlighting the importance of thermal gradients in current generation. The differences seen in figure 19 are consistent with what other studies have observed (see, for example, [24]).

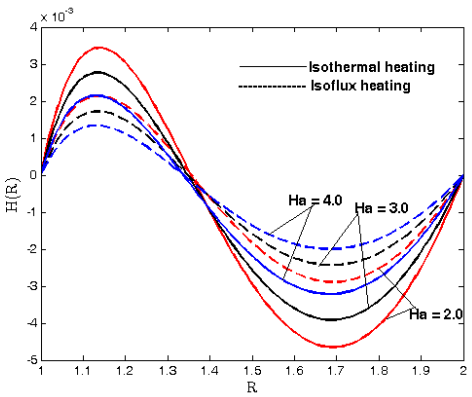


Figure 10: Magnetic field profile for different values of $Ha$ at $S = 0.5, N = 1, K^* = 1$ and $\lambda = 2$

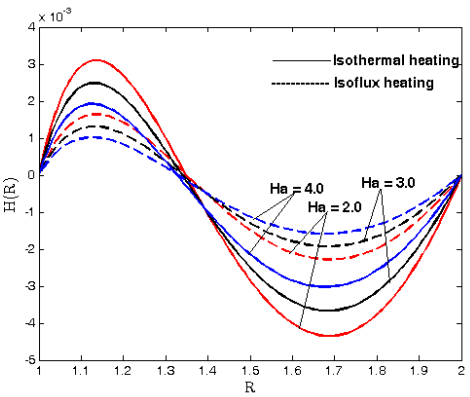


Figure 11: Magnetic field profile for different values of $Ha$ at $S = 4, N = 1, K^* = 1$ and $\lambda = 2$

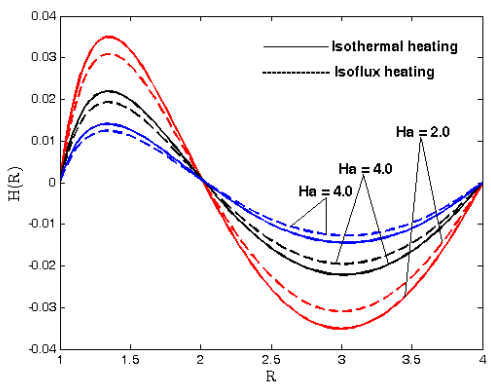


Figure 12: Magnetic field profile for different values of $Ha$ at $S = 1, N = 1, K^* = 1$ and $\lambda = 4$

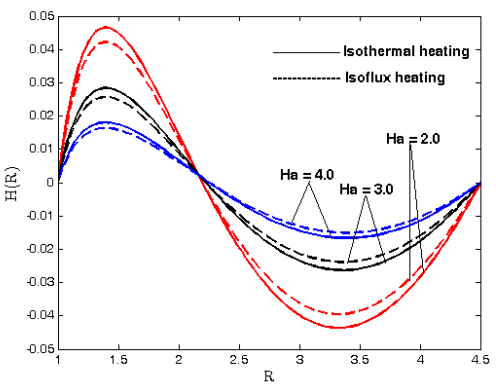


Figure 13: Magnetic field profile for different values of $Ha$ at $S = 1, N = 1, K^* = 1$ and $\lambda = 4.5$

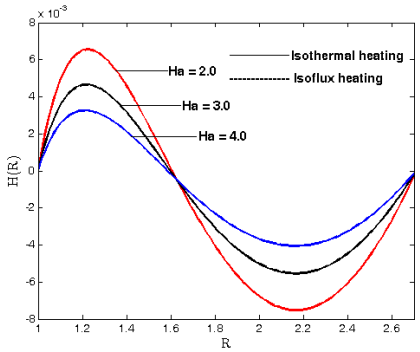


Figure 14: Magnetic field profile for different values of $Ha$ at $S \to 0, K^* \to 0, N = 0$ and $\lambda = 2.71$

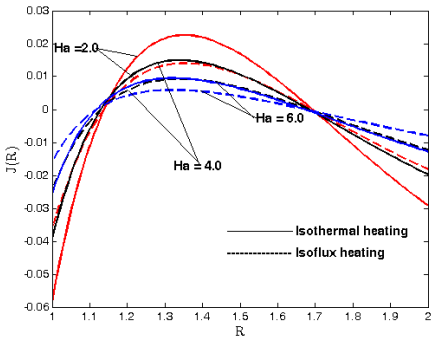


Figure 15: Induced Current density profile for different values of $Ha$ at $\lambda = 2, S = 0.5, N = 1.0$, and $K^* = 1$

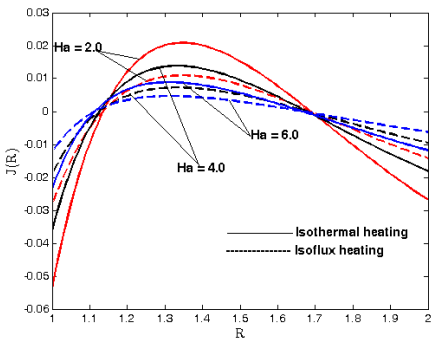


Figure 16: Induced Current density profile for different values of $Ha$ at $\lambda = 2, S = 4.0, N = 1.0$, and $K^* = 1$

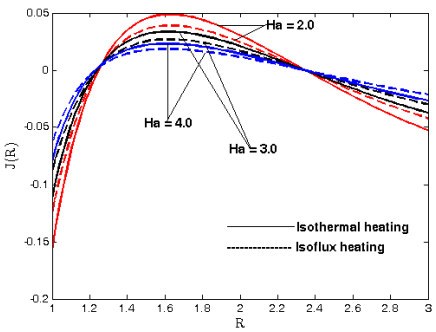


Figure 17: Induced Current density profile for different values of $Ha$ at $\lambda = 3, S = 1.0, N = 1.0$, and $K^* = 1.0$

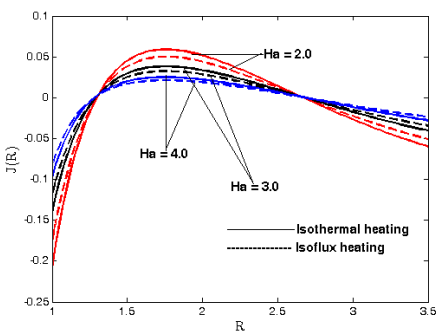


Figure 18: Induced Current density profile for different values of $Ha$ at $\lambda = 3.5, S = 1.0, N = 1.0$, and $K^* = 1.0$

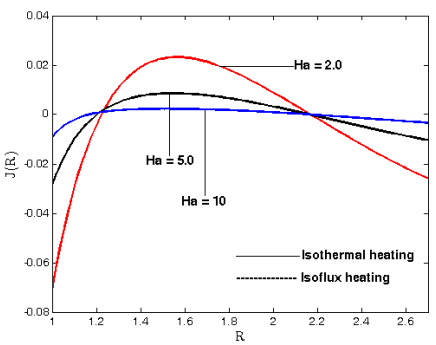


Figure 19: Induced Current density profile for different values of $Ha$ at $\lambda = 2.71, S =\to 0 N = 0$ and $K^* \to 0$

Table 1: Dimensionless Nusselt Numbers for Temperature and Thermal Flux Absorption

| $\lambda$ | $S$ | $\mathrm{Nu}_1$ (Isothermal) | $\mathrm{Nu}_\lambda$ (Isothermal) | $\mathrm{Nu}_1$ (Iso-flux) | $\mathrm{Nu}_\lambda$ (Iso-flux) |
|---|---|---|---|---|---|
| 1.80 | 1.00 | 1.8929 | 0.8929 | 1.0000 | 0.4717 |
| 1.80 | 2.00 | 2.0762 | 0.8445 | 1.0000 | 0.4067 |
| 2.00 | 1.00 | 1.6667 | 0.6667 | 1.0000 | 0.4000 |
| 2.00 | 2.00 | 1.8777 | 0.6176 | 1.0000 | 0.3289 |
| 2.50 | 1.00 | 1.3810 | 0.3810 | 1.0000 | 0.2759 |
| 2.50 | 2.00 | 1.6432 | 0.3347 | 1.0000 | 0.2037 |

Table 2: Dimensionless Sherwood Numbers for Both Isothermal and Iso-flux Conditions

| $\lambda$ | $K^*$ | $\mathrm{Sh}_1$ (Isothermal) | $\mathrm{Sh}_\lambda$ (Isothermal) | $\mathrm{Sh}_1$ (Iso-flux) | $\mathrm{Sh}_\lambda$ (Iso-flux) |
|---|---|---|---|---|---|
| 1.80 | 0.40 | 1.6222 | 0.9673 | 1.0000 | 0.5963 |
| 1.80 | 1.00 | 1.5007 | 1.0019 | 1.0000 | 0.6676 |
| 2.00 | 0.40 | 1.3491 | 0.7450 | 1.0000 | 0.5522 |
| 2.00 | 1.00 | 1.2039 | 0.7825 | 1.0000 | 0.6500 |
| 2.50 | 0.40 | 0.9664 | 0.4620 | 1.0000 | 0.4781 |
| 2.50 | 1.00 | 0.7673 | 0.5042 | 1.0000 | 0.6571 |

Table 3: Numerical values of dimensionless $\tau_1$, $\tau_\lambda$, $Q$, and induced current flux ($J$) for isothermal and iso-flux conditions for different values of $Ha$, $S$, and $\lambda$

| $Ha$ | $S$ | $\lambda$ | Isothermal | | | Iso-flux | | | $J$ | |
|---|---|---|---|---|---|---|---|---|---|---|
| | | | $\tau_1$ | $\tau_\lambda$ | $Q$ | $\tau_1$ | $\tau_\lambda$ | $Q$ | Isothermal | Iso-flux |
| 2 | 1 | 1.8 | 0.2387 | 0.0845 | 0.1347 | 0.1261 | 0.0447 | 0.0712 | 0.1092 | 0.0577 |
| 3 | 1 | 1.8 | 0.2151 | 0.0727 | 0.1167 | 0.1137 | 0.0384 | 0.0616 | 0.0462 | 0.0244 |
| 4 | 1 | 1.8 | 0.1907 | 0.0606 | 0.0982 | 0.1007 | 0.0320 | 0.0519 | 0.0235 | 0.0124 |
| 2 | 1 | 2 | 0.2859 | 0.0948 | 0.2570 | 0.1715 | 0.0569 | 0.1542 | 0.1244 | 0.0747 |
| 3 | 1 | 2 | 0.2494 | 0.0781 | 0.2133 | 0.1496 | 0.0469 | 0.1280 | 0.0512 | 0.0307 |
| 4 | 1 | 2 | 0.2144 | 0.0626 | 0.1722 | 0.1286 | 0.0376 | 0.1033 | 0.0254 | 0.0152 |
| 2 | 1 | 3 | 0.4599 | 0.1200 | 1.8060 | 0.3679 | 0.0960 | 1.4448 | 0.1800 | 0.0144 |
| 3 | 1 | 3 | 0.3530 | 0.0861 | 1.2815 | 0.2824 | 0.0689 | 1.0252 | 0.0656 | 0.0525 |
| 4 | 1 | 3 | 0.2755 | 0.0623 | 0.9123 | 0.2204 | 0.0498 | 0.7299 | 0.0298 | 0.0238 |
| 2 | 2 | 1.8 | 0.2330 | 0.0811 | 0.1298 | 0.1122 | 0.0390 | 0.0625 | 0.1153 | 0.0555 |
| 3 | 2 | 1.8 | 0.2102 | 0.0696 | 0.1124 | 0.1012 | 0.0335 | 0.0542 | 0.0476 | 0.0229 |
| 4 | 2 | 1.8 | 0.1865 | 0.0580 | 0.0947 | 0.0898 | 0.0280 | 0.0456 | 0.0240 | 0.0115 |
| 2 | 2 | 2 | 0.2765 | 0.0894 | 0.2442 | 0.1473 | 0.0476 | 0.1300 | 0.1306 | 0.0695 |
| 3 | 2 | 2 | 0.2416 | 0.0736 | 0.2025 | 0.1287 | 0.0392 | 0.1079 | 0.0525 | 0.0280 |
| 4 | 2 | 2 | 0.2082 | 0.0589 | 0.1635 | 0.1109 | 0.0314 | 0.0871 | 0.0258 | 0.0137 |
| 2 | 2 | 3 | 0.4256 | 0.1037 | 1.5894 | 0.2752 | 0.0670 | 1.0277 | 0.1826 | 0.1181 |
| 3 | 2 | 3 | 0.3296 | 0.0741 | 1.1261 | 0.2131 | 0.0479 | 0.7281 | 0.0657 | 0.0425 |
| 4 | 2 | 3 | 0.2595 | 0.0533 | 0.8004 | 0.1678 | 0.0344 | 0.5175 | 0.0297 | 0.0192 |

## 5. Comparison and Validation

Table 4: Comparison of Numerical values of fluid flux for isothermal and constant heat flux cases of this study and the study of [24] at $S \to 0$, $K^* = 0$ and $N = 0$

| Parameter | Current Study | Singh et al. | Difference | Error (%) |
|---|---|---|---|---|
| $\tau_1$ (Isothermal) | 0.26843 | 0.27016 | −0.00173 | −0.64 |
| $\tau_\lambda$ (Isothermal) | 0.10046 | 0.10142 | −0.00096 | −0.95 |
| $Q$ (Isothermal) | 0.15826 | 0.15943 | −0.00117 | −0.73 |
| $\tau_1$ (Iso-flux) | 0.15776 | 0.15880 | −0.00104 | −0.66 |
| $\tau_\lambda$ (Iso-flux) | 0.05904 | 0.05962 | −0.00058 | −0.97 |
| $Q$ (Iso-flux) | 0.09302 | 0.09371 | −0.00069 | −0.74 |

**Key Observations**

- **Excellent Agreement:** Differences are less than 1% for every measure, confirming that the current study is in line with previous research.
- **Consistent Trends:** Higher $\tau_1$, $\tau_\lambda$ and $Q$ for isothermal compared to isoflux heating
- **Hartmann Number Impact:** As Ha increases:
  - $\tau_1 \downarrow$ by 8.8% (both cases)
  - $Q \downarrow$ by 11.6% (both cases)
- **Validation:** The comparative analysis confirms strong agreement between both studies.

## 6. Conclusion

The study provides a comprehensive analytical investigation of MHD natural convection heat and mass transfer in a vertical concentric annulus influenced by applied radial and induced magnetic fields, along with inverse-square heat and mass absorption. The key findings are as follows:

- Increasing Ha decreases velocity because of the Lorentz force, but it also raises the strength of the magnetic field. The induced current density oscillates and stabilizes at larger Ha values because of electromagnetic resistance.
- The annular gap ($\lambda$) makes the flow of heat and mass more efficient by spreading out the temperature and speed more evenly. This effect is very important for applications that need good heat and mass transfer.
- The heat absorption parameter (S) is very important for getting energy out. When S values are higher, the speed and temperature go down. This shows that heat absorption removes thermal energy from the system. This effect is stronger when the annular gap is large.
- The rate of the chemical reaction ($K^*$) is very important in mass transport analysis. When $K^*$ goes up, the concentration goes down because chemical reactions get stronger and use up reactants faster.
- The buoyancy ratio parameter (N) changes the distribution of velocity and concentration. This shows how natural convection can assist in maintaining stable flow. This effect is useful in many fields, such a industry and the environment.
- The induced current flux (J) changes a lot depending on the situation, which shows that thermal and electromagnetic forces have a strong coupling.

- Isothermal boundary conditions result in higher Nusselt and Sherwood numbers than iso-flux conditions, signifying improved convective transport.

A possible solution to optimizing MHD-driven systems is to control parameters like Ha, S, $K^*$, and $\lambda$ to enhance thermal and mass transport in engineering applications such as nuclear reactor cooling and electromagnetic propulsion. The study also confirms that isothermal boundary conditions lead to more effective convective transport than iso-flux conditions.

The study suggests that future research should include non-Newtonian fluids, look into time-dependent effects, and look into how changing boundary conditions affect MHD convection systems in real-world engineering situations.

## References


1. Arora, K. L., & Gupta, P. R. (1972). Magnetohydrodynamic flow between two rotating coaxial cylinders under radial magnetic field. Physics of Fluids, 15(6), 1146–1148.
2. Chambre, P. L. (1957). The laminar boundary layer with distributed heat sources or sinks. Applied Science Research, Section A, 6(5), 393–401.
3. El-Shaarawi, M. A. I., & Sarhan, A. (1981). Developing laminar free convection in an open-ended vertical annulus with a rotating inner cylinder. ASME Journal of Heat Transfer, 103(3), 552–558.
4. Foraboschi, F. P., & Di Federico, I. (1964). Heat transfer in laminar flow of non-Newtonian heat-generating fluids. International Journal of Heat and Mass Transfer, 7(3), 315–325.
5. Gee, R. E., & Lyon, J. B. (1957). Non-isothermal flow of viscous non-Newtonian fluids. Industrial & Engineering Chemistry, 49(6), 956–960.
6. Inman, R. M. (1962). Experimental study of temperature distribution in laminar tube flow of a fluid with internal heat generation. International Journal of Heat and Mass Transfer, 5(11), 1053–1058.
7. Jha, B. K., & Ajibade, A. O. (2009). Free convective flow of heat generating/absorbing fluid between vertical porous plates with periodic heat input. International Communications in Heat and Mass Transfer, 36(6), 624–631.
8. Jha, B. K., Oni, M. O., & Aina, B. (2018). Steady fully developed mixed convection flow in a vertical micro-concentric-annulus with heat generating/absorbing fluid: An exact solution. Ain Shams Engineering Journal, 9(4), 1289–1301.
9. Jha, B. K., & Aina, B. (2018). Impact of induced magnetic field on magnetohydrodynamic natural convection flow in a vertical annular micro-channel in the presence of radial magnetic field. Propulsion and Power Research, 7, 171–181.
10. Joshi, H. M. (1987). Fully developed natural convection in an isothermal vertical annular duct. International Communications in Heat and Mass Transfer, 14(6), 657–664.
11. Kumar, D., & Singh, A. K. (2016). Effect of heat source/sink and induced magnetic field on natural convective flow in vertical concentric annuli. Alexandria Engineering Journal, 55, 3125–3133.
12. Madejski, J. (1963). Temperature distribution in channel flow with friction. International Journal of Heat and Mass Transfer, 6(1), 49–51.
13. Moalem, D. (1976). Steady state heat transfer within porous medium with temperature dependent heat generation. International Journal of Heat and Mass Transfer, 19(5), 529–537.
14. Muhammad, M. Y., Gambo, Y. Y., & Lawan, M. A. (2025). Effect of inverse-square heat absorption on MHD natural convection flow in a vertical concentric annulus with radial and induced magnetic fields. *Mechanical Engineering Advances*, 3(2), 2534. https://doi.org/10.59400/mea2534
15. Muhammad, M. Y., Gambo, Y. Y. U., & Lawan, M. A. (2025). Influence of Heat and Mass Generation on MHD Natural Convection Flow in a Vertical Concentric Annulus with Applied and Induced Magnetic Fields. *NIPES-Journal of Science and Technology Research*, 7(1), 290-310.
16. Muhammad, Y. M., Yusuf, Y. G., & Muhammad, A. L. (2024). Inverse-square heat generation effect on MHD natural convection flow in a vertical concentric annulus with radial and induced magnetic field. *Bayero Journal of Pure and Applied Sciences*, 15(1), 169-183.
17. Muhammad, Y. M., Lawan, M. A., & Gambo, Y. Y. (2024). Heat absorption effects of magneto-natural convection flow in vertical concentric annuli with influence of radial and induced magnetic field. Scientific Reports, 14, 15165.
18. Ostrach, S. (1954). Combined natural- and forced-convection flow and heat transfer of fluids with and without heat sources in channels with linearly varying wall temperatures. National Advisory Committee for Aeronautics, Technical Report NACA-TN-3141.
19. Oni, M. O. (2017). Combined effect of heat source, porosity, and thermal radiation on mixed convection flow in a vertical annulus: An exact solution. Engineering Science and Technology, an International Journal, 20(2), 518–527.

20. Oni, M. O., Jha, B. K., Abba, J. M., & Adebayo, O. H. (2024). Influence of radially varying magnetic fields and heat sources/sinks on MHD free-convection flow within a vertical concentric annulus. Power Engineering and Engineering Thermophysics, 3(1), 27–44.

21. Pollard, A., & Oosthuizen, P. (1983). Free convection through open-ended pipes. ASME, 105(10), 93.

22. Ramamoorthy, P. (1961). Flow between two concentric rotating cylinders with a radial magnetic field. Physics of Fluids, 4(11).

23. Rossow, V. J. (1958). On flow of electrically conducting fluids over a flat plate in the presence of a transverse magnetic field. NACA Technical Note, NACA-TR-1358.

24. Singh, R. K., & Singh, A. K. (2012). Effect of induced magnetic field on natural convection in vertical concentric annuli. Acta Mechanica Sinica, 28, 315–323.

25. Singh, S. K., Jha, B. K., & Singh, A. K. (1997). Natural convection flow in a vertical concentric annuli under a radial magnetic field. Heat and Mass Transfer, 32, 399–401.

26. Toor, H. L. (1956). The energy equation for viscous flow-effect of expansion on temperature profiles. Industrial & Engineering Chemistry, 48(5), 922–926.

27. Yusuf, S. T. (2017). Exact solution of an MHD natural convection flow in vertical concentric annulus with heat absorption. International Journal of Fluid Mechanics & Thermal Sciences, 3(5), 52–61.

## A. Appendix I: Constants

The constants used in the analytical solutions are defined as follows:

$$D_1 = [(2+\sqrt{S})^2 - Ha^2],\ D_2 = [(2-\sqrt{S})^2 - Ha^2],\ D_3 = -\frac{NC_7}{[(2+\sqrt{K^*})^2 - Ha^2]},\ D_4 = -\frac{NC_8}{[(2-\sqrt{K^*})^2 - Ha^2]},$$

$$D_5 = D_1 + D_2 + D_3 + D_4,\ D_6 = D_1\lambda^{(2+\sqrt{S})} + D_2\lambda^{(2-\sqrt{S})} + D_3\lambda^{(2+\sqrt{K^*})} + D_4\lambda^{(2-\sqrt{K^*})},$$

$$C_2 = \frac{D_5\lambda^{Ha} - D_6}{(\lambda^{-Ha} - \lambda^{Ha})},\ C_1 = -C_2 - D_5,\ C_5 = -\frac{\xi}{(\chi\sqrt{S}+\gamma) + (\chi\sqrt{S}-\gamma)\lambda^{2\sqrt{S}}},$$

$$C_6 = -\frac{\xi\lambda^{2\sqrt{S}}}{(\chi\sqrt{S}+\gamma) + (\chi\sqrt{S}-\gamma)\lambda^{2\sqrt{S}}},\ C_4 = D_{21},\ C_3 = \frac{D_{23} - D_{21}}{\ln(\lambda)},$$

$$C_7 = -\frac{\xi}{(\chi\sqrt{K^\circ}+\gamma) + (\chi\sqrt{K^\circ}-\gamma)\lambda^{2\sqrt{K^\circ}}},\ C_8 = -\frac{\xi\lambda^{2\sqrt{K'}}}{(\chi\sqrt{K'}+\gamma) + (\chi\sqrt{K'}-\gamma)\lambda^{2\sqrt{K'}}},$$

$$D_7 = D_1(2+\sqrt{S}) + D_2(2-\sqrt{S}),\ D_8 = D_3(2+\sqrt{K^*}) + D_4(2-\sqrt{K^*}),$$

$$D_9 = -[D_1(2+\sqrt{S})\lambda^{1+\sqrt{S}} + D_2(2-\sqrt{S})\lambda^{1-\sqrt{S}}],$$

$$D_{10} = -[D_3(2+\sqrt{K^*})\lambda^{1+\sqrt{K^*}} + D_4(2-\sqrt{K^*})\lambda^{1-\sqrt{K^*}}],$$

$$D_{11} = \frac{C_3}{2}(\lambda^2 - 1),\ D_{12} = \frac{D_1}{(4+\sqrt{S})}(\lambda^{4+\sqrt{S}} - 1),\ D_{13} = \frac{D_2}{(4-\sqrt{S})}(\lambda^{4-\sqrt{S}} - 1),$$

$$D_{14} = \frac{D_3}{(4+\sqrt{K^\circ})}(\lambda^{4+\sqrt{K^\circ}} - 1),\ D_{15} = \frac{D_4}{(4-\sqrt{K^\circ})}(\lambda^{4-\sqrt{K^\circ}} - 1),\ D_{16} = D_{11} + D_{12} + D_{13} + D_{14} + D_{15},$$

$$D_{17} = -\frac{D_1}{(2+\sqrt{S})},\ D_{18} = -\frac{D_2}{(2-\sqrt{S})},\ D_{19} = -\frac{D_3}{(2+\sqrt{K^*})},\ D_{20} = -\frac{D_4}{(2-\sqrt{K^*})},$$

$$D_{21} = \frac{C_1 - C_2}{Ha} + D_{17} + D_{18} + D_{19} + D_{20},\ D_{22} = D_{17}\lambda^{(2+\sqrt{S})} + D_{18}\lambda^{(2-\sqrt{S})} + D_{19}\lambda^{(2+\sqrt{K^\circ})} + D_{20}\lambda^{(2-\sqrt{K^\circ})},$$

$$D_{23} = \frac{(C_1\lambda^{Ha} - C_2\lambda^{-Ha})}{Ha} + D_{22},\ D_{24} = D_{17}(\lambda^{2+\sqrt{S}} - 1) + D_{18}(\lambda^{2-\sqrt{S}} - 1),$$

$$D_{25} = D_{19}(\lambda^{2+\sqrt{K^\circ}} - 1) + D_{20}(\lambda^{2-\sqrt{K^\circ}} - 1) - C_3\ln(\lambda)$$

## B. Appendix II: Nomenclature

**Roman Symbols:**

| Symbol | Description |
|---|---|
| a | Inner cylinder radius (m) |
| b | Outer cylinder radius (m) |
| g | Gravitational acceleration (m/s$^2$) |
| $H'_o$ | Applied magnetic field (A/m) |
| $H'_{z'}$ | Magnetic field induced in the z'-direction (A/m) |
| H | Dimensionless induced magnetic field in z-direction |
| $C_P$ | Specific heat at constant pressure (J/(kg•K)) |
| $J_\theta$ | Induced current density along $\theta$-direction (A/m$^2$) |
| Ha | Hartmann number (dimensionless) |
| $r', \theta', z'$ | Cylindrical coordinates (m) |
| R | Dimensionless radial distance |
| T' | Fluid Temperature (K) |
| $\theta$ | Dimensionless fluid temperature |
| $T'_a$ | Temperature of the surroundings (K) |
| $T'_i$ | Temperature of the inner cylinder at the surface (K) |
| U | Dimensionless velocity of the fluid along the axial direction |
| U' | Fluid velocity along the axial direction (m/s) |
| $U_o$ | Characteristic fluid velocity (m/s) |
| $Nu_1$ | Nusselt number at the inner cylinder (dimensionless) |
| $Nu_\lambda$ | Outer cylinder Nusselt number (dimensionless) |
| $Q_o$ | Rate of heat generation per unit volume (W/m$^3$) |
| S | Heat source/sink parameter (dimensionless) |
| $K^*$ | Chemical reaction parameter |
| N | Buoyancy ratio parameter |
| C | Concentration of the fluid |
| $\phi$ | Dimensionless concentration |

**Greek Symbols:**

| Symbol | Description |
|---|---|
| $\beta$ | Thermal expansion coefficient ($K^{-1}$) |
| $\beta^*$ | Solutal expansion coefficient ($m^3/kg$) |
| $k$ | Fluid thermal conductivity (W/(m•K)) |
| $\mu_e$ | Magnetic permeability (H/m) |
| $\nu$ | Fluid kinematic viscosity (m$^2$/s) |
| $\eta$ | Magnetic diffusivity (m$^2$/s) |
| $\rho$ | Fluid Density (kg/m$^3$) |
| $\lambda$ | Annular gap (dimensionless) |
| $\tau_1$ | Inner cylinder Skin friction coefficient (dimensionless) |
| $\tau_\lambda$ | Outer cylinder Skin friction coefficient (dimensionless) |

*M. Y. Muhammad,*
*Muhammad Auwal Lawan Mukhazah,*
*Department of Mathematics,*
*Aliko Dangote University of Science and Technology,*
*Wudil, 700101 Kano, Nigeria.*
*E-mail address:* muhammadyusufmuhammad@kustwudil.edu.ng and Mukhazah3@gmail.com

*and*

*Yusuf Y. Gambo,*

*Ado Balili,*
*Auwalu Alhassan Girema,*
*Department of Mathematics,*
*Yusuf Maitama Sule University Kano, Nigeria.*
*E-mail address:* yygambo@gmail.com, adobalili@gmail.com and Giremaguyuk4321@gmail.com